



# New status of the infrared beamlines at SSRF

Xiao-Jie Zhou<sup>1</sup> · Hua-Chun Zhu<sup>2</sup> · Jia-Jia Zhong<sup>1</sup> · Wei-Wei Peng<sup>2</sup> ·  
Te Ji<sup>2</sup> · Yue-Cheng Lin<sup>3,4</sup> · Yu-Zhao Tang<sup>1</sup> · Min Chen<sup>2</sup>

Received: 24 July 2019 / Revised: 12 September 2019 / Accepted: 14 September 2019 / Published online: 21 November 2019  
© China Science Publishing & Media Ltd. (Science Press), Shanghai Institute of Applied Physics, the Chinese Academy of Sciences, Chinese Nuclear Society and Springer Nature Singapore Pte Ltd. 2019

**Abstract** There are two infrared beamlines at the Shanghai synchrotron radiation facility (SSRF)—BL01B and BL06B. BL01B was the first infrared beamline of the National Facility for Protein Science in Shanghai at SSRF, which is dedicated to synchrotron infrared microspectroscopy. It utilizes bending magnet radiation and edge radiation as light sources. Diffraction-limited spatial resolution is reached in the infrared microspectroscopy experiment. BL01B has been in operation for approximately five years since it opened in January 2015. In the past few years, many meaningful results have been published by user groups from various disciplines, such as biomacromolecule materials and pharmaceutical, environmental, and biomedical sciences. In addition, a new infrared

beamline station BL06B is under construction, which is optimized for the mid-infrared and far-infrared band. BL06B is equipped with a vacuum-type Fourier transform infrared spectrometer, infrared microscope, custom long-working-distance infrared microscope, infrared scanning near-field optical microscope, and mid-infrared Mueller ellipsometer. The purpose is to serve experiments with high vacuum requirements and spatial resolution experiments, as well as those that are in situ and time-sensitive, such as high-pressure and atomic force microscopy infrared experiments. The station can be used for research in biomaterials, pharmacy, geophysics, nanotechnology, and semiconductor materials.

**Keywords** Synchrotron radiation · Fourier transform infrared spectroscopy · Infrared microspectroscopy · Infrared beamlines

This work was supported by the National Natural Science Foundation of China (Nos. U1732130, U1632273, 11505267, and 11605281).

Xiao-Jie Zhou and Hua-Chun Zhu have contributed equally to this work.

✉ Yu-Zhao Tang  
tangyuzhao@sari.ac.cn

✉ Min Chen  
chenmin@sinap.ac.cn

<sup>1</sup> National Facility for Protein Science in Shanghai, Shanghai Advanced Research Institute, Chinese Academy of Sciences, Shanghai 201210, China

<sup>2</sup> Shanghai Synchrotron Radiation Facility, Shanghai Advanced Research Institute, Chinese Academy of Sciences, Shanghai 201210, China

<sup>3</sup> Shanghai Institute of Applied Physics, Chinese Academy of Sciences, Shanghai 201800, China

<sup>4</sup> University of Chinese Academy of Sciences, Beijing 100049, China

## 1 Introduction

Infrared spectroscopy is one of the most important analytical tools that is widely used in biology, chemistry, physics, and materials science. Based on the outstanding brightness, focusability, polarization, and tunability of synchrotron infrared radiation, dozens of infrared beamlines have been built at synchrotron facilities around the world [1, 2]. The most prominent advantage of synchrotron infrared radiation is its brightness; it is two to three orders of magnitude brighter than the conventional IR source. This renders it more powerful to study heterogeneous samples noninvasively and with higher spatial resolution. Coupled with infrared microscopy, synchrotron radiation (SR) infrared microspectroscopy can reach diffraction-

limited resolution and achieve high S/N ratios, even when the aperture size is below 20  $\mu\text{m}$  [3, 4]. SR infrared microspectroscopy has been widely used in biology, macromolecular materials, chemistry, and high-pressure, environmental, and pharmaceutical sciences. Based on its pulse polarization properties and wide spectral range, it is also suited to study dynamic processes and systems that need varying photon energies or wavelengths [1].

SSRF is an intermediate-energy third-generation light source that provides a wide spectral range from the far-infrared to hard X-ray regions [5]. There are currently 15 beamlines in operation at SSRF. Only one of them is based on SR infrared light, which is the infrared microspectroscopy beamline BL01B. Another infrared beamline, BL06B, is also under construction and will soon be open to users. The construction of BL01B started in 2010 under the collaboration of NFPS and SSRF. It was commissioned and opened to users in 2015. The SR infrared light source, Fourier transform infrared spectrometer, and infrared microscope are combined, and theoretical diffraction-limited resolution is achieved. BL01B was originally aimed at studying protein science and biology. To meet the demands from different research areas, the beamline is now open to users from various disciplines. Construction on BL06B started in 2016, with plans to be commissioned and open to users in 2020. BL06B is optimized for the mid-infrared and far-infrared bands, equipped with a vacuum-type Fourier transform infrared (FTIR) spectrometer, infrared microscope, custom long-working-distance infrared microscope, infrared scanning near-field optical microscopy (SNOM) instrument, and a mid-infrared Mueller ellipsometer (MIME), aimed at used for research in biomaterials, pharmacy, geophysics, nanotechnology, and semiconductor materials. In this paper, the beamline layout and endstation of the BL01B and BL06B is briefly introduced. The applications of BL01B are summarized and updated.

## 2 Infrared microspectroscopy beamline: BL01B

### 2.1 Beamline overview

SSRF is a third-generation light source based on a storage ring with the beam energy of 3.5 GeV. The top-up mode is now in operation for users, with the beam current of 240 mA. Both bending magnet radiation (BMR) and edge radiation (ER) are extracted from the storage ring as the infrared light source of BL01B. The extraction solid angles in the horizontal and vertical directions are 40 mrad ( $-15$  to 25 mrad) and 20 mrad ( $-10$  to 10 mrad), respectively. The detailed design and layout have been previously reported [6]. A brief overview of the optical layout of BL01B is introduced. As shown in Fig. 1, plane

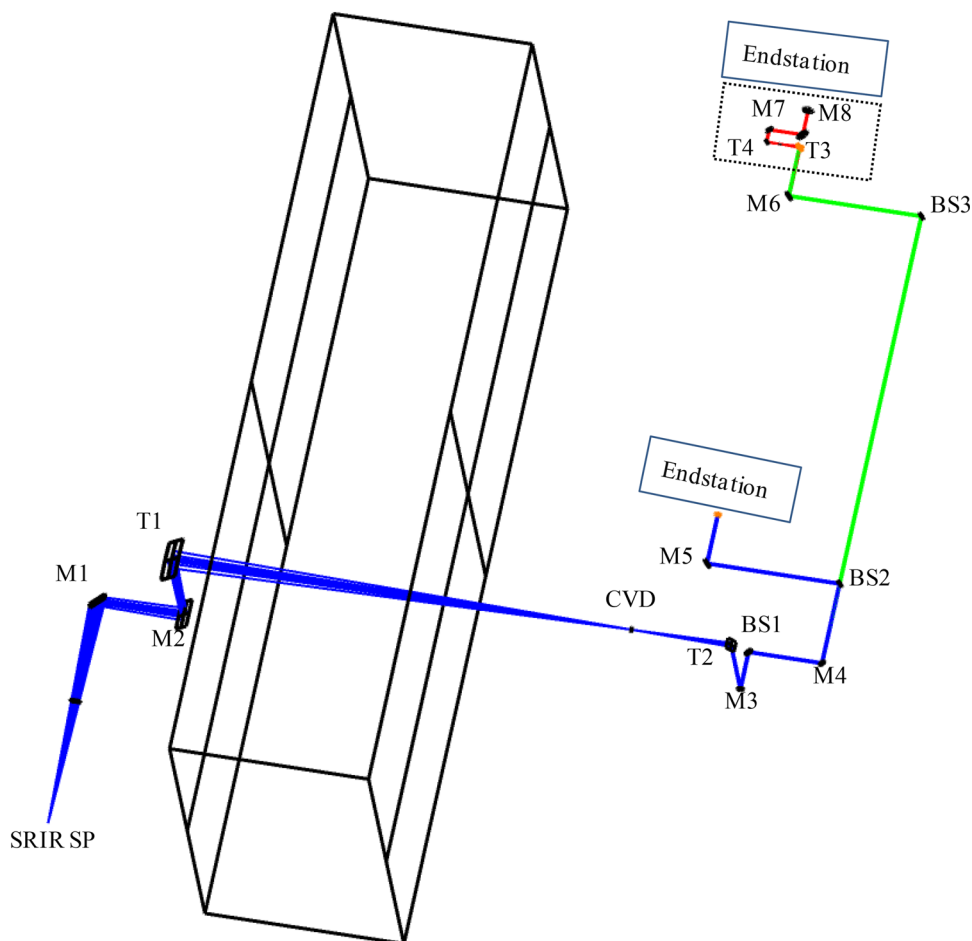
mirror M1 is the extraction mirror, which is slotted in the middle to allow high-energy X-ray and UV radiation to pass through. As reported before, M1 is angled at  $45^\circ$  to the axis of the incident light, such that it reflects the photo beam horizontally [6]. The photo beam is reflected by M1 to a plane mirror M2 and then reflected by M2 to a toroidal-focusing mirror T1. T1 directs the photo beam through a hole in the tunnel wall, then through a CVD diamond window that separates the ultra-high vacuum section from the downstream high vacuum section. The photo beam goes through a variable slit that blocks the stray light coming from the upstream optics. Toroidal mirror T2 directs the beam to plane mirror M3, beam splitter BS1, and plane mirror M4. BS2 is used to control which experiment station receives the beam. BS1 and BS3 reflect the infrared light and transmit visible light. An active feedback system was installed after T2, which includes M3, M4, BS1, BS2, and BS3 [6, 7]. The feedback system of the accelerator has worked well since 2015, and the electron beam orbit is quite stable; thus, the system has not been in operation since then. Plane mirrors M5 and M6 are used to direct the photo beam to different endstations. The control system of the beamline is based on EPICS from the Linux operation system.

Recently, to increase the photon flux transmission efficiency, a pair of off-axis parabolic mirrors is added in front of the spectrometer. By adjusting the magnification of the off-axis parabolic mirrors, the collimated beam size incident on the microscope is changed to match the numerical aperture of the  $15\times$  and  $32\times$  objective lenses of the microscope to improve the photon flux transmission efficiency. The collimating beam size after plane mirror M6 is  $\sim 50 \times 20 \text{ mm}^2$ , while the aperture size of the  $15\times$  and  $32\times$  condensers are 10 mm and 6.5 mm, respectively. Thus, the photon flux transmission efficiency can be improved by adjusting the collimating beam size to theoretically match the aperture size of the condenser. The detailed optical path is shown in the dashed box in Fig. 1 and can be described as below. The photo beam is reflected by M6 to off-axis parabolic mirror T3. Then, the focused beam is reflected and collimated by another off-axis parabolic mirror T4 to plane mirror M7. Finally, the collimated photo beam is reflected by plane mirror M8 to the entrance of the spectrometer.

### 2.2 Endstation

Based on the above-mentioned beamline, BL01B is mainly used to conduct infrared microspectroscopy experiments. The main instruments are a Nicolet 6700 FTIR spectrometer and a Nicolet Continuum infrared microscope. The Nicolet Continuum infrared microscope is equipped with a  $10\times$  visible objective,  $15\times$  [NA (Numerical Aperture) = 0.58] IR/visible objective, and  $32\times$  (NA = 0.65) IR/visible objective. The

**Fig. 1** (Color online) Simple schematic optical layout of BL01B at SSRF. M1, M2, M3, M4, M5, M6, M7, M8: plane mirror; T1, T2: toroidal mirror; T3, T4: off-axis parabolic mirror; BS1, BS2, BS3: IR/Vis beam splitter



working distance of the  $15\times$  objective is 11 mm, and the working distance of the  $32\times$  objective is 7 mm. An optional slide-on attenuated total reflection (ATR) accessory is available for the  $15\times$  objective. Mercury cadmium telluride (MCT/A) with liquid  $N_2$  cooled and thermoelectricity cooled (TEC) InGaAs detectors are installed in the Continuum infrared microscope. The MCT/A detector is used for the  $600\text{--}11,700\text{ cm}^{-1}$  region. The TEC InGaAs detector is used for the  $3800\text{--}12,000\text{ cm}^{-1}$  region. The Nicolet 6700 FTIR spectrometer is also equipped with MCT/A with a liquid  $N_2$  cooled detector, deuterated triglycine sulfate (DTGS) w/KBr detector (with KBr window), DTGS w/PE detector (with PE window), and MCT/B with a liquid  $N_2$  cooled detector. The DTGS w/KBr (with KBr window) detector is used for the  $350\text{--}12,500\text{ cm}^{-1}$  region. The DTGS w/PE detector (with PE window) is used for the  $10\text{--}700\text{ cm}^{-1}$  region. The MCT/B detector is used for the  $400\text{--}11,700\text{ cm}^{-1}$  region.  $CaF_2$ , KBr, and PE beam splitters are optional for near-, mid-, and far-infrared experiments, respectively. The  $CaF_2$  beam splitter is used for the  $4000\text{--}15,500\text{ cm}^{-1}$  region, KBr beam splitter is used for the  $350\text{--}7800\text{ cm}^{-1}$  region and PE beam splitter is used for the  $30\text{--}680\text{ cm}^{-1}$  region. A Nicolet 8700 FTIR spectrometer is also available. This spectrometer is equipped

with a Si bolometer with a helium-cooled detector and a photodiode MCT detector. The Si bolometer with helium-cooled detector is used for  $10\text{--}370\text{ cm}^{-1}$  region, and the photodiode MCT detector is used for the  $650\text{--}11,700\text{ cm}^{-1}$  region. The beam splitters are versatile for both spectrometers. The infrared microscope and spectrometers are purged with dry air and a purge gas generator to reduce water and carbon dioxide absorption from the atmosphere. Various universal accessories are available for both spectrometers, such as a liquid cell, micro-compression diamond cell kit, Smart iTR, and sample shuttle.

As listed in Table 1, for the infrared microspectroscopy station, the spectral range covers  $600\text{--}10,000\text{ cm}^{-1}$ , with an optimal spectral resolution of  $0.1\text{ cm}^{-1}$ . The photon flux at the entrance of the spectrometer is  $1.9 \times 10^{13}$  photon  $s^{-1}$  per 0.1% band width at  $1\text{ }\mu\text{m}$ , 300 mA. The measurement and calculation methods of the photo flux at the entrance of the spectrometer have been introduced in a previous study [8]. The focused spot diameter at  $1000\text{ cm}^{-1}$  is  $18\text{ }\mu\text{m}$  (for the  $32\times$  objective,  $NA = 0.65$ ), for which the diffraction limit reaches  $\sim 18.8\text{ }\mu\text{m}$  [6, 8]. The spatial resolution of the infrared microscope is in good agreement with the theoretical diffraction-limited

**Table 1** Performance of the infrared microspectroscopy endstation

Spectral range	600–10,000 $\text{cm}^{-1}$
Spectral resolution	0.1 $\text{cm}^{-1}$
Photon flux (at entrance of the spectrometer)	$1.9 \times 10^{13}$ photon $\text{s}^{-1}$ per 0.1% b.w. at 1 $\mu\text{m}$ , 300 mA
Focused spot size	$\sim 18 \mu\text{m}$ at 1000 $\text{cm}^{-1}$ (diffraction-limited resolution)
Minimum aperture size	$5 \times 5 \mu\text{m}^2$
Control precision of the automatic sample stage	1 $\mu\text{m}$

resolution [6, 8]. When the aperture size is smaller than  $15 \times 15 \mu\text{m}^2$ , the signal-to-noise ratio (SNR) of synchrotron infrared radiation is two orders of magnitude better than that of the globar light source in the spectrometer. For example, when the aperture size is  $5 \times 5 \mu\text{m}^2$ , the SNR of the synchrotron infrared radiation is approximately 350 times better than that of the globar light source [6, 8]. When the aperture size is below  $50 \times 50 \mu\text{m}^2$ , the intensity in arbitrary units of the peak-to-peak interferogram values of the synchrotron radiation is much higher than that of the globar light source. The control precision of the automatic sample stage is 1  $\mu\text{m}$ .

The software OMNIC and Atl $\mu$ s are used for experimental setup, data collection, and data processing. A commercial version of Cytospec is also available upon request for analyzing vibrational hyperspectral imaging data sets. OMNIC can be used to perform basic data processing, such as baseline correction, smoothing, normalization to a specific band, and differentiation. Atl $\mu$ s can be used to collect and process mapping data, including creating “chemigram,” “peak height of one peak,” and “peak height ratio of two peaks” profiles. Atl $\mu$ s can also be used to reprocess a map file, such as truncating the spectral and spatial ranges of a map, extracting a line map from an area map, and correcting map spectra. Cytospec is a program specifically used to analyze vibrational spectroscopic imaging data sets, such as those from IR and Raman imaging. Except for spectral and spatial preprocessing, Cytospec can be used to perform univariate imaging analysis and multivariate statistical imaging analysis. The multivariate methods of data analysis include principal component analysis (PCA), hierarchical cluster analysis (HCA), and k-means cluster imaging (KMC). The “Series” function that is a part of OMNIC software is also available, and it can be used to collect a group of spectra at set intervals.

### 2.3 Experiment modes and methods

Three experiment modes are available to choose from for an infrared microspectroscopy study—transmission, transfection, and ATR modes [9]. Simple schematics of these experimental modes are shown in Fig. 2. In transmission mode, the sample is usually placed on substrates that are transparent to both infrared light and visible light, such as

barium fluoride ( $\text{BaF}_2$ ) and calcium fluoride ( $\text{CaF}_2$ ). When infrared light passes through the sample and substrate, the spectrum of the sample can be measured. In transfection mode, the sample is usually placed on an inexpensive IR-reflecting surface, such as low-emissivity slides. Infrared measurements are generated by a beam passing through the sample and reflecting back from the substrate through the sample. In ATR mode, the sample is in contact with an internal reflection element (IRE) with a high refractive index. The IR beam is directed through the IRE, and the evanescent wave extends beyond the IRE surface, penetrating the sample [9]. Then, the FTIR spectra of the sample are recorded. The infrared microscope is also equipped with an optional wire-grid infrared polarizer. The infrared polarizer can be used for both transmission and transfection experiments to obtain information that is specific to the sample orientation. A point spectrum can be collected to study a specific sample point of interest with high spatial resolution. Mapping can be collected point-by-point to study a sample area of interest with high spatial resolution. Series spectra can also be collected at set intervals.

To keep the beam current stable in the storage ring, the accelerator periodically injects the electron beam into the storage ring (when accelerator is working in top-up mode). Spectrum noise is introduced by the fluctuating disturbances of the beam current. To eliminate the noise introduced in top-up mode, a trigger device based on a network is developed to detect the beam current change in the storage ring of the SSRF [10]. The sampling of the FTIR spectrometer is suspended when the electron beam is injected into the storage ring, and the sampling is resumed after the injection is completed. In addition, a zone median filter method is proposed to reduce the noise level introduced in top-up mode, while FTIR spectrometer operates in the rapid scan mode, the experimental results show that the spectrum noise can be reduced greatly, and the spectral SNR can be improved using this method [11].

Owing to its high brightness and high collimation performance, the infrared microspectroscopy station is especially suitable for 3D infrared experiments. A 3D CT experiment was carried out with synchrotron infrared radiation as the illumination source at the BL01B infrared microspectroscopy station, and project mapping was achieved with point-by-point scanning method. The 3D

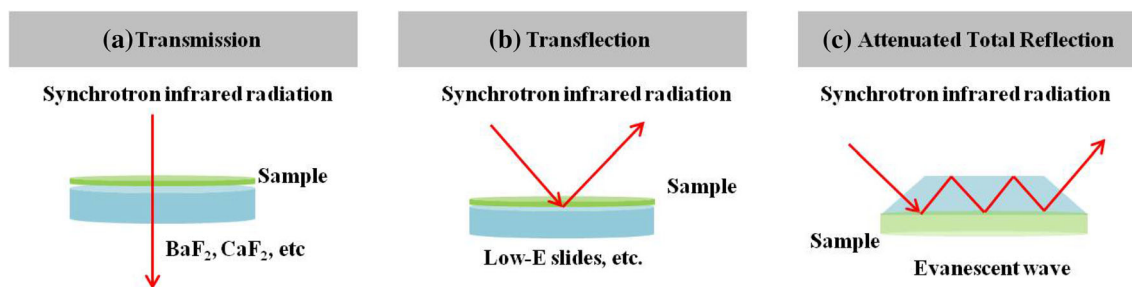


**Fig. 2** (Color online) Simple schematic of **a** transmission mode, **b** transflection mode, and **c** ATR mode

data were already reconstructed, and good results were obtained. After further optimization of the design and algorithm, it can be opened to users. Details of these experiments will be reported in a future publication.

An infrared microfluidic device is developed at BL01B to study live biosystems at the single-cell level. Microfluidic devices can be used not only to control water thickness precisely, but also to provide a hospitable environment for live biosystems. Combining synchrotron infrared radiation and microfluidic devices, various biosystems can be studied, such as live cells, microbial systems, and biofluid. The custom synchrotron infrared microfluidic system includes a microfluidic chip, syringe pump, and temperature-control sample stage. The system has been tested at BL01B and is being optimized. Further opening it to users is planned. Details regarding this device will be reported in a future publication.

## 2.4 Ancillary facility

The BL01B beamline offers support for end users to prepare samples. BL01B is equipped with instruments such as a tablet press, Leica freezing microtome, Leica vibratome, paraffin slicing machine, stereomicroscope, ultrasonic apparatus, centrifuge, and vacuum drying apparatus. Basic sample treatment reagents are available, such as ultra-pure water, ethyl alcohol, optimal cutting temperature (OCT) compound for freezing microtome, paraffin, and potassium bromide (KBr). A Linkam FTIR600 heating stage is available to be coupled with the infrared microscope, providing temperature control from  $-196$  to  $600$  °C.

## 3 New infrared beamline in phase II project: BL06B

### 3.1 Beamline overview

The extraction angle of the infrared beam line is limited by the secondary magnet on the storage ring, as the extraction angle of the BL06B is the same as that of the BL01B. The schematic of the optical layout is shown in

**Fig. 3.** Plane mirror M1 is the extraction mirror, with a larger slot width in the middle than that used by BL01B to allow the high-energy X-ray and UV radiation to pass through. The infrared beam is reflected by M1 to plane mirror M2, which is outside the tunnel, then reflected by M2 to toroidal mirror T1. The infrared beam is focused by T1 and passed through the CVD diamond window, which is used to isolate the ultra-high vacuum section and high vacuum of the downstream section. Then, the infrared beam is reflected by T2 to plane mirror M3. Owing to the limited angle of the extraction, an asymmetric optical structure was adopted. In this structure, the object distance to image distance ratio of T1 is set to 2.4. Because of the large object distance to image distance ratio of the toroidal mirror T1, additional aberrations were introduced. Thus, a toroidal mirror, T2, was placed behind the CVD diamond window with the same T1 parameters used to correct the aberration. The purpose of the design is to compress the spot size of the far infrared on the CVD diamond window to improve the transmission efficiency of the far infrared and reduce the light intensity loss of the spectral segment due to the carbon peak absorption of the diamond CVD [12]. Plane mirror M4 is a switching mirror, which is used to control the direction of the beamline. When M4 moves outside the light path, the infrared beam goes through a variable slit that blocks the stray light coming from the upstream optics. Then, the infrared beam is reflected by plane mirror M5a to off-axis parabolic mirror T3a, which is used as a collimating mirror. Plane mirror M6a is a switching mirror similar to M4. When M6a is outside the optical path, the collimated infrared beam travels to the AFM-IR station. When M6a is in the optical path, the collimated infrared beam is reflected by M6a to off-axis parabolic mirror T4a and then focused by T4a to the microspectroscopy station, which is equipped with a Bruker Vertex 80v FTIR spectrometer and Hyperion 3000 infrared microscope. When M4 moves into the optical path, the infrared beam is reflected by plane mirror M5b to toroidal mirror T3b, then directed by T3b to plane mirror M6b; then, it is reflected by M6b to toroidal mirror T4b, directed by T4b to plane mirror M7b, and reflected by M7b

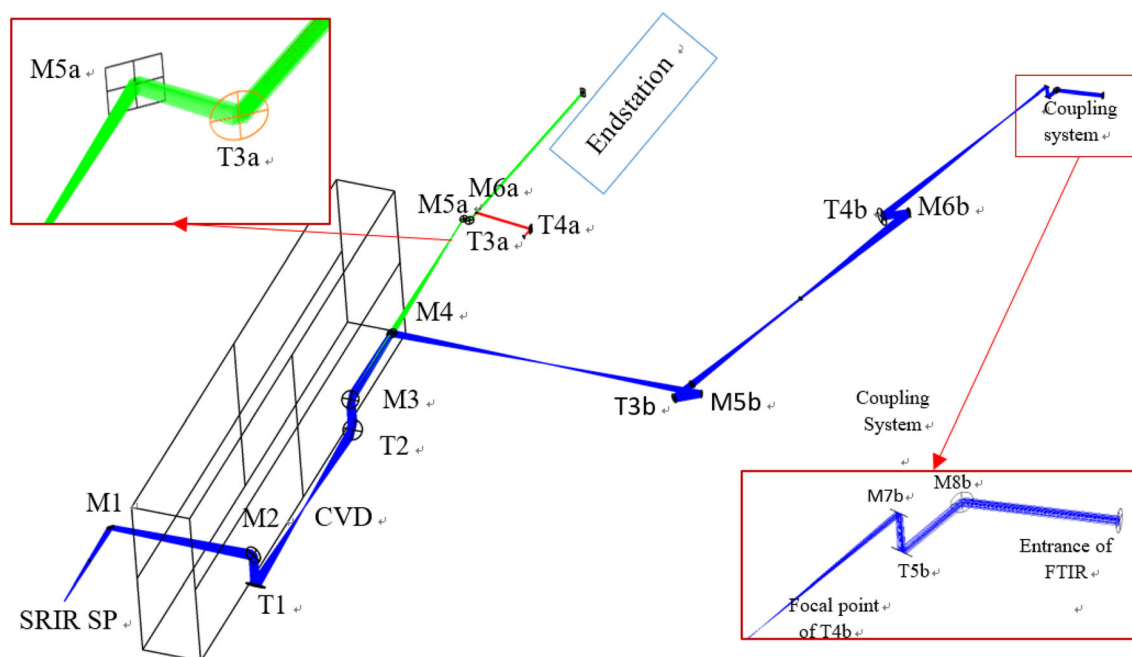


**Fig. 3** (Color online) 3D schematic optical layout of BL06B at SSRF. M1–M4, M5a, M6a, M5b, M6b, M7b, M8b: plane mirror; T1–T2, T3b–T5b: toroidal mirror; T3a, T4a, T5b: off-axis parabolic mirror

to off-axis parabolic mirror T5b. Finally, it is collimated by T5b, reflected to plane mirror M8b, and then reflected by M8b to the FTIR spectrometer of the ED-XAS and IR combined experimental station.

### 3.2 Endstation

#### 3.2.1 Infrared station of BL06B

Based on the above-mentioned beamline, BL06B is mainly used for spectroscopy and experimental microspectroscopy with high vacuum requirements, nanoscale spectroscopy, and infrared polarization spectroscopy.

Infrared SNOM can detect samples in different ways, such as reflection and transmission [13]. It can analyze and characterize nanomaterials and realize nondestructive imaging of chemical components at the nanoscale. Using synchrotron radiation as the light source, the high-intensity and wide-spectrum characteristics of the synchrotron radiation source can be fully utilized, and sample information with high SNR can be obtained. This technology has very broad application prospects in the field of nanomaterials, such as in photonic crystals, waveguides, organic semiconductor materials, polymer materials, and organic solar cells.

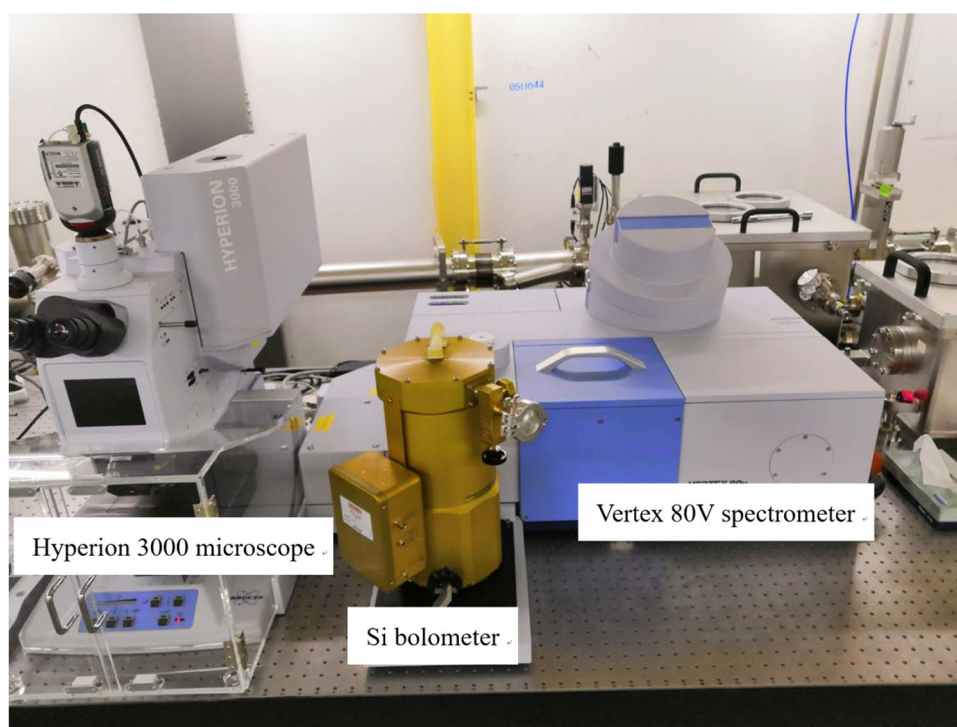
In addition, the MIME can be used to analyze the change in polarized light reflected by the sample, complex refractive index, or dielectric tensor of the sample [14]. The

spectral range of the MIME is  $800\text{--}2500\text{ cm}^{-1}$  when working with the Vertex 80v FTIR spectrometer.

The infrared station of BL06B is equipped with a vacuum-type Bruker Vertex 80v FTIR spectrometer and Hyperion 3000 infrared microscope (Bruker, Germany), which is shown in Fig. 4. The spectral range of the FTIR spectrometer is  $10\text{--}10,000\text{ cm}^{-1}$ , with a resolution better than  $0.1\text{ cm}^{-1}$ , wavenumber accuracy better than  $0.01\text{ cm}^{-1}$ , transmittance accuracy better than  $0.1\%$  T, and SNR higher than  $60,000:1$  (peak-to-peak). It is equipped with a millisecond-level fast-sweep function (110 spectra/s) and equipped with  $\text{CaF}_2$ , KBr, and Mylar beam splitters and InGaAs, DTGS, MCT, and Si bolometer detectors.

The main accessories of FTIR spectrometer are variable-temperature ATR cell, low-temperature control cell, variable-angle reflectance accessory, diffuse reflection cell, and high-temperature and high-pressure cell. The variable-temperature ATR unit is suitable for measuring the infrared spectrum of solids, liquids, films, and soft materials as a function of temperature. The crystal in the ATR unit accessory is a diamond, and the temperature change is controlled by the software program. The low-temperature control cell can realize a program temperature control of  $-269.15$  to  $51.85\text{ }^\circ\text{C}$  and can be used for infrared transmission spectrum measurement at low temperature. It is suitable for studying the infrared optical properties of condensed materials, such as superconducting materials, semiconductor films, and nano-oxides, at low temperature. The high-temperature and high-pressure cell can control

**Fig. 4** (Color online) Infrared microspectroscopy (Hyperion 3000 microscope, Si bolometer, and Vertex 80 V spectrometer, from Bruker, Germany)



the temperature up to 800 °C, pressure up to 66 bar, and vacuum as low as  $10^{-1}$  Torr. The sample can be measured by FTIR in transmission or reflection mode under different temperature and atmospheric conditions, which is suitable for studying the reaction and catalytic mechanisms and various in situ reaction processes. The variable-angle reflectance accessory can be used to obtain a spectrum of any flat, reflecting surface on plate or sheet material. Measurements of the reflectance are useful in the quality control of optical materials and to obtain information regarding the crystalline structure of a material. The variable-angle reflectance accessory can be used to obtain reflection spectra of dielectrics at optimum angle and reflection–absorption and refractive index spectra of thin films.

The spectral range of the Bruker Hyperion 3000 infrared microscope is  $600\text{--}8000\text{ cm}^{-1}$ , which is determined by the detector used by this microscope. The spatial resolution of the stage used in the microscopy analysis is approximately  $1\text{ }\mu\text{m}$ . The sampling modes of infrared microscopy include transmission, transfection, ATR, and GIR. The main accessories of the infrared microscope are as follows: ATR and GIR objectives, heating and cooling stages for microscopy, and diamond compression cell. The GIR objective of the Bruker is unique. In the objective, the IR beam passes through the sample twice for better sensitivity. The GIR objective can be used to measure very thin coatings on metallic substrates, which often requires the grazing angle incidence reflection to improve the interaction of the IR beam with the sample. The GIR objective can

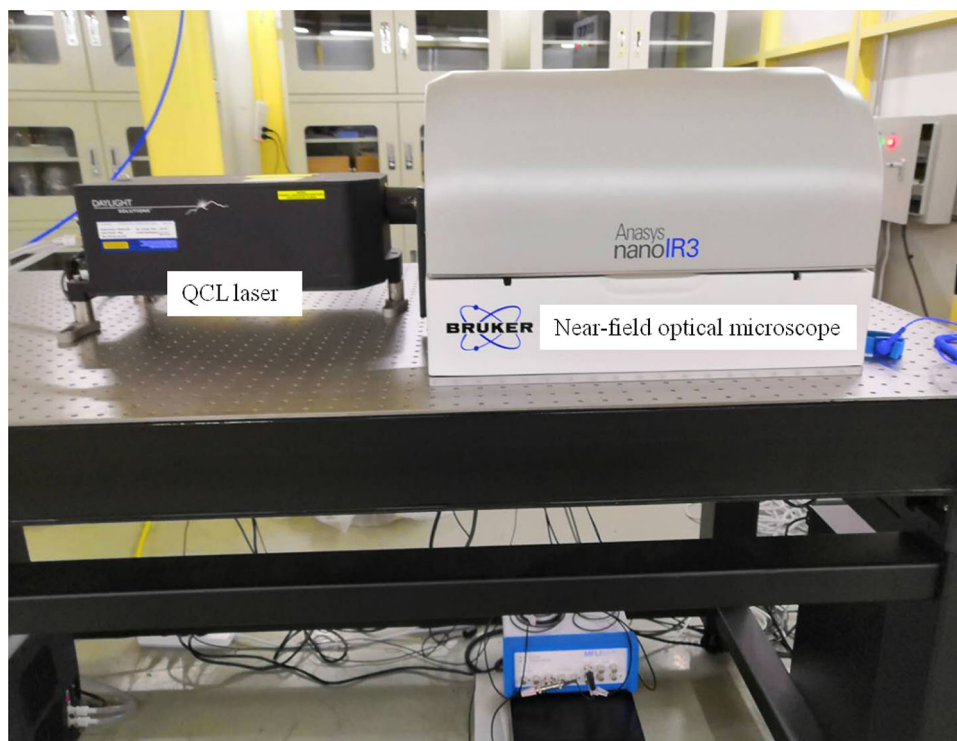
achieve the highest level of sensitivity while retaining the polarization characteristics of the infrared beam.

The experimental station is also equipped with an Anasys nanoIR3-s SNOM system (from Bruker, Germany), which can achieve near-field intensity and phase-synchronized imaging with a spatial resolution of several tens of nanometers in the visible, near-infrared, and mid-infrared bands. The SNOM system is shown in Fig. 5. It provides a new nanoscale analytical tool for research in nanomaterials, semiconductors, biology, and chemistry. The SNOM instrument is equipped with four QCL laser chips, which can work in the Pulse or Pulse/CW mode; the range of each chip is approximately  $90\text{--}110\text{ cm}^{-1}$ . The center wavenumber of these four chips is in the range of  $1000\text{--}1610\text{ cm}^{-1}$ . The SNOM system can be used for s-SNOM and AFM-IR measurements. The SNOM system is equipped with an external interface and optical mirror system to use with the external infrared source provided by the synchrotron radiation infrared (SRIR) beamline. The SNOM instrument must also be used to perform an s-SNOM and AFM-IR experiment with the external SRIR source. With the SRIR source, the SNOM system can cover the  $900\text{--}4000\text{ cm}^{-1}$  spectral range.

### 3.2.2 ED-XAS and IR combined experimental station

This experimental station will focus on the ED-XAS and IR combined experiments. The latter are mainly used to study the structure–activity relationship of the catalytic reaction process and conduct dynamic in situ monitoring of the catalyst and catalytic processes (such as catalyst atomic

**Fig. 5** (Color online) Anasys nanoIR3-s near-field optical microscope (from Bruker, Germany)



electronic structure, surface reaction molecules, and products), understand the catalytic mechanism from the atomic molecular level, achieve reaction direction selection and control, and regulate reaction products.

The infrared part of the combined experimental station is equipped with a custom long-working-distance infrared microscope, which has a working distance of approximately 80 mm; it is used for coupling the infrared beam and X-ray beam onto the same sample point. This special custom microscope works in conjunction with the vacuum-type Bruker Vertex 80v FTIR spectrometer; the spectral range of this FTIR spectrometer is 100–10,000  $\text{cm}^{-1}$ , with a resolution better than 0.1  $\text{cm}^{-1}$ , wavenumber accuracy better than 0.01  $\text{cm}^{-1}$ , transmittance accuracy better than 0.1% T, and SNR higher than 60,000:1 (peak-to-peak). It is equipped with a millisecond-level fast-sweep function (110 spectra/s),  $\text{CaF}_2$ , KBr, and Mylar beam splitters, and InGaAs, DTGS, MCT, and Si bolometer detectors. More details regarding this experimental station will be reported in a future publication.

#### 4 Applications of the BL01B infrared microspectroscopy beamline

Synchrotron infrared microspectroscopy is an outstanding technique to study small samples and sample areas with diffraction-limited spatial resolution. User groups of BL01B come from various backgrounds, such as biomacromolecule

materials and pharmaceutical, environmental, biomedical, and high-pressure sciences. Commissioned in 2015, BL01B has entered its fifth year of operation. BL01B provides approximately 4000 h of user time per year. The beam time includes that for general users, urgent proposals, reward for publications, and cooperation time of users with beamline. In the future, business and other significant proposals may also be arranged according to demand. The number of articles published increases every year. Previous user publications have been introduced before [15]. A series of studies has been conducted by Fang et al. [16] to study animal silks and regenerated silk fibroin (RSF) fibers using BL01B. Microscopic structures of silk fibers have been studied, and their relationship with the mechanical properties of silk fibers has been built. BL01B has also been used to study pharmaceutical science by Jiwen Zhang et al., such as the hydration-induced material transfer in membranes of osmotic pump tablets and the characterization of the protein/peptide distribution in single microspheres [17, 18]. In environmental science, BL01B has been used to study the binding and interactions of heavy metals with functional groups in soils by Sun et al. [19]. In biological science, BL01B has been used by Liu et al. [20] to study the early adipogenic differentiation of human mesenchymal stem cells at the single-cell level, discrimination of bacteria, and molecular changes in bacteria. In high-pressure science, organic–inorganic hybrid perovskite materials have been studied by Lingping Kong et al. using BL01B [21, 22].

In this section, we update some new applications of BL01B in the past two years, showing that synchrotron infrared microspectroscopy can be used to investigate a wide range of scientific issues. Biomacromolecule materials and pharmaceutical, environmental, and biomedical sciences are still the main fields that are focused on by BL01B user groups.

SR infrared microspectroscopy is a powerful technique to study the secondary structures of silk fibroins, especially at the single silk fibroin level because of the high brightness of the SR. BL01B has been widely used in this area. Tensan silk-inspired hierarchical fibers have been studied by Zhang et al. [23], and their applications in smart textile have been explored. The structure transition of *Antheraea pernyi* silk fiber induced by contraction has been studied by Wang et al. [24]. The modification of silk fiber by mechanical properties has been examined by Liu et al. [25]. In the above-mentioned works, the microscopic structures and silk fibroin conformations have been investigated by using BL01B. Mesostructures in silk fibers are closely related to their mechanical performance and functions, and these mesostructures include microfibrils, nanofibrils, and nanoparticles. Isolation of silk mesostructures has been studied by Zheng et al. [26], and the applications of these mesosilks in electronic and environmental fields were explored. Mapping of *N. pseudonarcissus* bulb slices was collected at BL01B to study the distribution of RhB/silk and RhB, demonstrating that SR infrared microspectroscopy is also a useful technique for studying chemical distributions in plant tissue with high spatial resolution.

In pharmaceutical science, BL01B has been frequently used by Jiwen Zhang et al. to study cyclodextrin-related systems [27–30]. Cyclodextrins (CDs) are usually used as multifunctional drug carriers in modern drug delivery systems. The fabrication of  $\beta$ -cyclodextrin and sialic acid copolymer and the biofunctionalization of  $\beta$ -cyclodextrin nanosponges have been studied [27, 28]. Nanoclusters in the nano-cages of  $\gamma$ -cyclodextrin metal–organic frameworks (CD-MOF) have also been examined [29, 30]. The organic-molecular structures and their functional groups in these CD-related compounds have been studied using SR infrared spectroscopy. These results prove that BL01B is well suited for studying structures and chemical compositions of drug samples.

In environmental science, BL01B is usually used to study the distributions of organic matter and functional groups in soils nondestructively. Studying the soil mineral-organic associations (MOAs) is of great importance for understanding soil carbon storage. MOAs have been studied by Xiao et al. [31], using SR infrared microspectroscopy in combination with two-dimensional FTIR correlation spectroscopy (2DCOS). This study provides a new and systematic strategy for studying the heterogeneous

distribution of ingredients in soils at the microscale. Zn is an important micronutrient in soils and plants. However, Zn deficiency is a serious problem in China cultivated soils. The binding characters and fate of Zn in soils have been studied by Sun et al. [32]; SR infrared microspectroscopy provided useful information of functional groups in soils with micrometer spatial resolution. Understanding the bacterial inhibition mechanism of natural minerals in soil is challenging and meaningful for soil carbon storage. Mechanism of iron minerals inhibiting the growth of *Pseudomonas brassicacearum* J12 has been studied by the same group, which offers further insights into soil carbon storage [33]. The binding microenvironments in the intact soil microaggregates have also been studied [34]. A combined methodology to assess the heterogeneous binding microenvironments between the mineral assemblages and biopolymers has been built, involving SR infrared microspectroscopy,  $\mu$ -XRF, and 2DCOS. These works provide new insight into the study on the agriculture and environment.

In biomedical science, BL01B is mainly used to study the structure and distribution of biomacromolecules. The content and distributions of the extracellular matrix in decellularized book-shaped bioscaffolds have been studied by Zhou et al. [35] SR infrared microspectroscopy was used to confirm that decellularization had a significant effect on the content and distributions of collagen and proteoglycan in fibrocartilage bioscaffolds. Studying the fibrocartilage regeneration is essential for promoting bone-tendon healing. A book-shaped acellular fibrocartilage scaffold has been prepared and studied by the same group, and the loading property of its seeding cells and chondrogenic inducibility were analyzed [36]. The content and distributions of GAGs and collagen were determined by SR infrared microspectroscopy. When nanoparticles interact with proteins under a biological environment, their chiral properties play a rather important role. The adsorption behaviors of bovine serum albumin (BSA) onto chiral surfaces of nanoparticles were studied by Wang et al. [37]. The BSA conformation was determined by using BL01B. This study provides a molecule-level understanding of protein corona on chiral surfaces, which is important for the biological effects of nanochirality in living organisms.

BL01B has also been used in the analysis of cultural heritage preservation. The ceiling paintings in Donghua Men, which is the east entrance gate of the Forbidden City [38], have been studied by using BL01B's synchrotron infrared microspectroscopy. The results exhibit distinct differences in the two types of panels painted in different periods, from painting techniques to material composition. The materials of fabric-on-paper panels are similar to those seen in Chinese scroll paintings. The technique of synchrotron radiation-based Fourier transform infrared

microspectroscopy offers a powerful analytical platform to obtain the material composition distribution of complex systems at micrometer resolution.

## 5 Discussion and perspective

The infrared beamline BL01B provides diffraction-limited spatial resolution for infrared microspectroscopy experiments. Transmission, transfection, and the ATR experiment can be performed by the BL01B. The beamline optics and endstation configuration are being optimized constantly to offer a stronger and more stable signal. During its operation in the past few years, publications of user work are increasing. BL01B is well suited for studying biomacromolecule materials and pharmaceutical, environmental, and biomedical sciences. In addition, a new infrared beam line station BL06B is present, which is optimized for the mid-infrared and far-infrared band, equipped with vacuum FTIR, infrared microscope, custom long-working-distance infrared microscope, infrared SNOM, and MIME. It can be used for experiments requiring high vacuum and space resolution, as well as in situ, time-sensitive experiments, such as high-pressure experiments and atomic force microscope infrared (AFM-IR) experiments. The station can be used for research in biomaterials, pharmaceuticals, geophysics, nanotechnology, and semiconductor materials. It is expected that BL06B will be in commission and open to users in 2020, which will promote the applications of SR infrared technique in various disciplines.

## References

- M.C. Martin, U. Schade, P. Lerch et al., Recent applications and current trends in analytical chemistry using synchrotron-based Fourier-transform infrared microspectroscopy. *TrAC, Trends Anal. Chem.* **29**, 453–463 (2010). <https://doi.org/10.1016/j.trac.2010.03.002>
- P. Dumas, F. Polack, B. Lagarde et al., Synchrotron infrared microscopy at the French synchrotron facility SOLEIL. *Infrared Phys. Technol.* **49**, 152–160 (2006). <https://doi.org/10.1016/j.infrared.2006.01.030>
- D. Creagh, J. Mckinlay, P. Dumas, The design of the infrared beamline at the Australian synchrotron. *Vib. Spectrosc.* **75**, 1995–1999 (2006). <https://doi.org/10.1016/j.vibspec.2006.02.009>
- H.Y. Holman, H.A. Bechtel, Z. Hao et al., Synchrotron IR spectromicroscopy: chemistry of living cells. *Anal. Chem.* **82**, 8757–8765 (2010). <https://doi.org/10.1021/ac100991d>
- M.H. Jiang, X. Yang, H.J. Xu et al., Shanghai synchrotron radiation facility. *Chin. Sci. Bull.* **54**, 4171–4181 (2009). <https://doi.org/10.1007/s11434-009-0689-y>
- T. Ji, Y.J. Tong, H.C. Zhu et al., The status of the first infrared beamline at Shanghai synchrotron radiation facility. *Nucl. Instrum. Methods A* **788**, 116–121 (2015). <https://doi.org/10.1016/j.nima.2015.03.080>
- T. Scarvie, N. Andresen, K. Baptiste et al., Noise reduction efforts for the ALS infrared beamlines. *Infrared Phys. Technol.* **45**, 403–408 (2004). <https://doi.org/10.1016/j.infrared.2004.01.009>
- Z. Zhang, M. Chen, Y. Tong et al., Performance of the infrared microspectroscopy station at SSRF. *Infrared Phys. Technol.* **67**, 521–5250 (2014). <https://doi.org/10.1016/j.infrared.2014.09.015>
- M.J. Baker, J. Trevisan, P. Bassan et al., Using Fourier transform IR spectroscopy to analyze biological materials. *Nat. Protoc.* **9**, 1771–1791 (2014). <https://doi.org/10.1038/nprot.2014.110>
- Y.J. Tong, M. Chen, T. Ji et al., A system and a method of eliminating the effect of top-up mode on the synchrotron infrared beamline. *China. CN 104390704*. 2016-05-11. (in Chinese)
- H.C. Zhu, Y.J. Tong, T. Ji et al., Elimination technology of noise introduced by top-up injection in synchrotron radiation infrared beamline. *J. Infrared Millim Waves* **37**, 251–256 (2018). <https://doi.org/10.11972/j.issn.1001-9014.2018.02.019> (in Chinese)
- H.C. Zhu, Y.J. Tong, T. Ji et al., Optimized design for synchrotron radiation infrared beamline with small extraction angle. *Acta Opt. Sin.* **36**, 1122002 (2016). <https://doi.org/10.3788/AOS201636.1122002>
- A. Dazzi, R. Prazeres, F. Glotin et al., Local infrared microspectroscopy with subwavelength spatial resolution with an atomic force microscope tip used as a photothermal sensor. *Opt. Lett.* **30**, 2388–2390 (2005). <https://doi.org/10.1364/OL.30.002388>
- J. Kircher, R. Henn, M. Cardona et al., Far-infrared ellipsometry using synchrotron radiation. *J. Opt. Soc. Am. B* **14**, 705–712 (1997). <https://doi.org/10.1364/JOSAB.14.000705>
- X. Zhou, J. Zhong, J. Dong et al., The BL01B1 infrared beamline at Shanghai synchrotron radiation facility. *Infrared Phys. Technol.* **94**, 250–254 (2018). <https://doi.org/10.1016/j.infrared.2018.09.013>
- G. Fang, Y. Tang, Z. Qi et al., Precise correlation of macroscopic mechanical properties and microscopic structures of animal silks—using *Antheraea pernyi* silkworm silk as an example. *J. Mater. Chem. B* **530**, 6042–6048 (2017). <https://doi.org/10.1039/C7TB01638G>
- L. Wu, X.Z. Yin, Z. Guo et al., Hydration induced material transfer in membranes of osmotic pump tablets measured by synchrotron radiation based FTIR. *Eur. J. Pharm. Sci.* **84**, 132–138 (2016). <https://doi.org/10.1016/j.ejps.2016.01.020>
- M. Wang, X. Lu, X. Yin et al., Synchrotron radiation-based Fourier-transform infrared spectromicroscopy for characterization of the protein/peptide distribution in single microspheres. *Acta Pharm. Sin. B* **53**, 270–276 (2015). <https://doi.org/10.1016/j.apsb.2015.03.008>
- F.S. Sun, M.L. Polizzotto, D. Guan et al., Exploring the interactions and binding sites between Cd and functional groups in soil using two-dimensional correlation spectroscopy and synchrotron radiation based spectromicroscopies. *J. Hazard. Mater.* **326**, 18–25 (2017). <https://doi.org/10.1016/j.jhazmat.2016.12.019>
- Z.X. Liu, Y.Z. Tang, F. Chen et al., Synchrotron FTIR microspectroscopy reveals early adipogenic differentiation of human mesenchymal stem cells at single-cell level. *Biochem. Biophys. Res. Commun.* **478**, 1286–1291 (2016). <https://doi.org/10.1016/j.bbrc.2016.08.112>
- L.P. Kong, G. Liu, J. Gong et al., Simultaneous band-gap narrowing and carrier-lifetime prolongation of organic-inorganic trihalide perovskites. *Proc. Natl. Acad. Sci. USA* **113**, 8910–8915 (2016). <https://doi.org/10.1073/pnas.1609030113>
- G. Liu, J. Gong, L.P. Kong et al., Isothermal pressure-derived metastable states in 2D hybrid perovskites showing enduring

- bandgap narrowing. Proc. Natl. Acad. Sci. USA **115**, 8076–8081 (2018). <https://doi.org/10.1073/pnas.1809167115>
23. W. Zhang, C. Ye, K. Zheng et al., Tensan silk inspired hierarchical fibers for smart textile applications. ACS Nano **12**, 6968–6977 (2018). <https://doi.org/10.1021/acsnano.8b02430>
  24. Y. Wang, J. Wen, B. Peng et al., Understanding the mechanical properties and structure transition of *Antheraea pernyi* silk fibre induced by its contraction. Biomacromolecules **19**, 1999–2006 (2018). <https://doi.org/10.1021/acs.biomac.7b01691>
  25. Q. Liu, X. Wang, X. Tan, X. Xie et al., A strategy for improving the mechanical properties of silk fiber by directly injection of ferric ions into silkworm. Mater. Des. **146**, 134–141 (2018). <https://doi.org/10.1016/j.matdes.2018.03.005>
  26. K. Zheng, J. Zhong, Z. Qi et al., Isolation of silk mesostructures for electronic and environmental applications. Adv. Funct. Mater. (2018). <https://doi.org/10.1002/adfm.201806380>
  27. P. Singh, X. Ren, Y. He et al., Fabrication of  $\beta$ -cyclodextrin and sialic acid copolymer by single pot reaction to site specific drug delivery. Arab. J. Chem. (2017). <https://doi.org/10.1016/j.arabjc.2017.11.011>
  28. P. Singh, X. Ren, T. Guo et al., Biofunctionalization of  $\beta$ -cyclodextrin nanosponges using cholesterol. Carbohydr. Polym. **190**, 23–30 (2018). <https://doi.org/10.1016/j.carbpol.2018.02.044>
  29. Y. He, W. Zhang, T. Guo et al., Drug nanoclusters formed in confined nano-cages of CD-MOF: dramatic enhancement of solubility and bioavailability of azilsartan. Acta. Pharm. Sin. B **9**, 97–106 (2018). <https://doi.org/10.1016/j.apsb.2018.09.003>
  30. J. Xu, L. Wu, T. Guo et al., A “Ship-in-a-Bottle” strategy to create folic acid nanoclusters inside the nanocages of  $\gamma$ -cyclodextrin metal-organic frameworks. Int. J. Pharm. **556**, 89–96 (2019). <https://doi.org/10.1016/j.ijpharm.2018.11.074>
  31. J. Xiao, Y. Wen, G. Yu et al., Strategy for microscale characterization of soil mineral-organic associations by synchrotron-radiation-based FTIR technology. Soil Sci. Soc. Am. J. **82**, 1583–1591 (2018). <https://doi.org/10.2136/sssaj2018.05.0211>
  32. F.S. Sun, G.H. Yu, M.L. Polizzotto et al., Toward understanding the binding of Zn in soils by two-dimensional correlation spectroscopy and synchrotron-radiation-based spectromicroscopies. Geoderma **337**, 238–245 (2019). <https://doi.org/10.1016/j.geoderma.2018.09.032>
  33. H.Y. Du, G.H. Yu, F.S. Sun et al., Iron minerals inhibit the growth of *Pseudomonas brassicacearum* J12 via a free-radical mechanism: implications for soil carbon storage. Biogeosciences **16**, 1433–1445 (2019). <https://doi.org/10.5194/bg-16-1433-2019>
  34. J. Xiao, Y.L. Wen, S. Dou et al., A new strategy for assessing the binding microenvironments in intact soil microaggregates. Soil Tillage Res. **189**, 123–130 (2019). <https://doi.org/10.1016/j.still.2019.01.008>
  35. Y.C. Zhou, C. Chen, Z. Guo et al., SR-FTIR as a tool for quantitative mapping of the content and distribution of extracellular matrix in decellularized book-shape bioscaffolds. BMC Musculoskelet. Dis. **19**, 220 (2018). <https://doi.org/10.1186/s12891-018-2149-9>
  36. C. Chen, F. Liu, Y. Tang et al., Book-shaped acellular fibrocartilage scaffold with cell-loading capability and chondrogenic inducibility for tissue-engineered fibrocartilage and bone-tendon healing. ACS Appl. Mater. Interfaces. **113**, 2891–2907 (2019). <https://doi.org/10.1021/acsami.8b20563>
  37. X. Wang, X. Wang, M. Wang et al., Probing adsorption behaviors of BSA onto chiral surfaces of nanoparticles. Small **14**, 1703982 (2018). <https://doi.org/10.1002/smll.201703982>
  38. Macro to Micro, *Examining Architectural Finishes* (Archetype, London, 2018), ISBN: 9781909492608